# Improving Neuron Stimulation Efficency by Altering Electrode Geometry

A. Ghazavi[1], D. Westwick[1], C. Luk[2], N. I. Syed[2] and C. Dalton[1]
[1]*Department of Electrical and Computer Engineering, University of Calgary, Calgary, Alberta, Canada*
[2]*Department of Anatomy and Cell Biology, University of Calgary, Calgary, Alberta, Canada*

Keywords: Neuron-electrode Interface, Neuron Stimulation, Sealing Resistance, Finite Element Model, Micro Electrode Array.

Abstract: Microelectrode arrays (MEA) are non-invasive tools for recording brain cell activity and have been successfully applied to a variety of neurons. However, MEAs fail where consistent stimulation of neurons is desired over an extended period of time. Here, a model is presented to study features that provide optimum stimulation threshold from different sizes and shapes of electrodes. Both simulation and *in vitro* experimental results suggest that star-shaped electrodes enable a threshold voltage that is 25% lower than that of an electrode with a circular shape, and are thus considered more efficient for neuronal stimulation. These findings are important as they will help produce more efficient microelectrode arrays for *in vivo* applications such as prosthetic devices, as well as for long-term *in vitro* neuron stimulation for studying neuronal networks and function.

## 1 INTRODUCTION

Stimulating microelectrode arrays are the basis for neuroprosthetic devices such as cochlear and retinal implants, bladder prostheses, upper and lower limb prosthetics as well as treatments for neurological disorders such as nerve regeneration electrodes, deep brain stimulation and vagus nerve stimulation (Cogan, 2008). Electrodes used for neuron stimulation should be able to stimulate the neurons for a long time period without causing neural damage (Rutten, 2002). Efficient power consumption of the electrode is also an important feature to be considered in their design (Wei and Grill, 2009). In order to optimize the neuron stimulation to achieve physiological levels of stimulation, it is necessary to design a more effective neuron-electrode junction. Several models have been used to investigate different approaches for improving an individual neuron-electrode interface. Investigations have considered: the effect of complete and defect sealing on sealing resistance and stimulus transfer; the effect of cell size on membrane depolarization (Buitenweg et al., 1999); the effects of neuron eccentricity; sealing gap size, and both cell and microelectrode radius for circular microelectrodes smaller than the cell on passive membrane depolarization (Buitenweg et al., 2003); the effects of anodic and catodic current stimuli on cell excitation for a circular microelectrode larger than the cell (Schoen and Fromherz, 2008) and the efficiency of high-perimeter planar electrodes for exciting axons (Wei and Grill, 2009).

In the present research, the electric field pattern for different planar microelectrode dimensions and shapes was investigated, in order to optimize the electrode geometry and to obtain the largest electric field within a cell. Our research shows that shapes with sharp edges and longer perimeters result in higher electric fields and sealing resistances.

## 2 MATERIALS AND METHODS

### 2.1 Experimental Methods

Neurons were experimentally stimulated by a microelectrode array and their responses were measured using sharp electrodes. The lowest stimulation amplitude which caused an action potential was compared between the different electrode designs.

Ghazavi A., Westwick D., Luk C., Syed N. and Dalton C..
Improving Neuron Stimulation Efficency by Altering Electrode Geometry.
DOI: 10.5220/0004238900510056
In *Proceedings of the International Conference on Biomedical Electronics and Devices* (BIODEVICES-2013), pages 51-56
ISBN: 978-989-8565-34-1

### 2.1.1 Planar Electrodes

Electrolyte/SU8/Au/Cr electrodes were used in this research. Electrodes are fabricated onto 1mm glass, with 10nm chrome and 150nm gold (Figure 1). The electrodes are covered with 0.5µm SU-8, which is patterned to have holes through the SU-8 to the star electrodes. The SU-8 layer aids physical location of the cell. The star-shaped electrodes are made in three different sizes with areas of approximately 280$\mu m^2$, 478$\mu m^2$ and 798$\mu m^2$ and perimeters of approximately 106µm, 148µm and 186µm (Figure 2), respectively. On each chip, there were three star shaped electrodes, each one with a *Lymnaea stagnalis* neuron, left pedal dorsal1 (LPeD1), cultured on it.


Figure 1: Cross section of one electrode.

Figure 2: Star electrodes with LPeD1 neurons cultured on them. The distance between electrodes is 100µm.

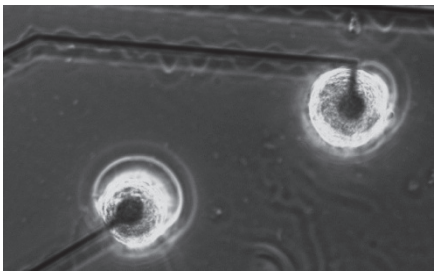

Figure 3: Circular electrodes with LPeD1 neuron cultured on them.

Conventional circular electrodes, 30µm in diameter were used for comparison purposes (Figure 3). The area and perimeter of the circular electrodes was 707$\mu m^2$ and 94µm, respectively. Four neurons were cultured onto four different circular electrodes. The electrodes were set at a distance of 100µm from each other.

### 2.1.2 Neurons

Neurons were extracted from isolated *Lymnaea Stagnalis* brains. The cell culture process was done according to previously published protocols as described by Syed et al. (1999). The cells were cultured on the electrodes which had been coated with poly-L-Lysine one day prior to the stimulation experiments.

## 2.2 Finite Element Modelling

An individual neuron-electrode interface has been modelled using the electric current mode of COMSOL 4.3(COMSOL Inc, USA), a Finite Element Modelling (FEM) software package. The transient FEM was developed in three-dimensions to model neuronal response in the subthreshold region. The model was meshed with 772014 and 622573 tetrahedral mesh elements for the star and circular electrodes, respectively. Poisson equation was solved numerically via FEM.

$$\nabla.(\sigma \nabla V) = 0 \qquad (1)$$

V the electrical potential and σ is the medium conductivity. The model includes an insulating surface around the glass. A falling voltage ramp with a slope of -60mV/ms in the duration of 10ms has been applied to the electrode. The passive response of neurons to subthreshold voltage ramp stimulations was compared for different electrodes. Since the membrane as well as the sealing gap and electrode double layer have small thicknesses compared to the other dimensions of the model, they have been modelled with a thickness larger than their actual thickness and their conductivity and permittivity have been compensated for the difference, as described by Buitenweg et al. (1999) and Choie and You (2012).

The level of discretization was validated by comparing both denser and coarser meshes.

### 2.2.1 Microelectrode

Several models have been proposed to represent the electrode-electrolyte impedance. There are two processes at the interface; faradaic and non-faradaic. In this research it has been assumed that there is no faradaic current at the gold-extracellular interface so the charge-transfer resistance and Warburg impedance have not been implemented in this model. Capacitive charging of the electrode double layer (DL) has been assumed to be the source of neuron stimulation. These currents are produced by the electrode double layer which acts as a capacitor. The pseudo capacitive resistance is assumed to be purely capacitive so:

$$Z = k(i\omega)^{-\beta} \quad ; \beta=1 \text{ , } k=1/C \tag{2}$$

In this work, the value 15μF/$cm^2$ as reported in literature, has been used for electrode impedance (Huang et al., 2004); (Yúfera et al., 2003). In reality the electrode DL is about 2nm (Huang *et al.,* 2004). Since meshing very thin layers in FEM is computationally costly, in the model a higher thickness 0.5μm has been considered and the difference is implemented in the permittivity.

$$\varepsilon_{DL} = c_{DL}.t_{implemented} \tag{3}$$

### 2.2.2 Neuron

The neuron was simulated as a paraboloid shape with radius 30μm and height 20μm (height≈0.7*radius). Variation of the height of neuron has a very small effect on stimulus transfer (Buitenweg et al., 1999). Since passive membrane properties have been assumed in the model, capacitive and resistive properties of the membrane are implemented in the model. Since a membrane's capacitance is inversely related to its thickness, which has a constant value for animal cells (Molleman, 2003), we have considered the value1μF/$cm^2$, as reported in other literature (Choi and You, 2012); (Molleman, 2003); (Huang et al., 2004); (Moulin et al., 2008); (Elia et al., 2009); (Buitenweg et al., 2003); (Schoen and Fromherz, 2007) for membrane specific capacitance.

The resistive properties of the membrane were represented by its conductivity. Right Pedal Dorsal1 (RPeD1) neuron's electrophysiology and size is almost the same as those of Left Pedal Dorsal1 (LPeD1) neuron, so the conductivity of RPeD1, 10nS (Lu and Feng, 2011), was used. The conductance and relative permittivity for the intracellular medium was considered to be 1.43S/m and 80, respectively. Due to the small thickness of the membrane, 8 nm (Huang et al., 2004), a large number of mesh elements was required. So it has been modelled as an interface layer between the intracellular and extracellular media (Choi and You, 2012).

$$\sigma_{model} = \sigma_{membrane}.t_{implemented} \tag{4}$$

$$\varepsilon_{membrane} = c_{membrane}.t_{implemented} \tag{5}$$

The gap between the cell and electrode is in reality around 50nm (Schoen and Fromherz, 2008), which was implemented as 0.5μm in the model, and then compensated for by using a higher conductivity.

$$\sigma_{gap} = \sigma_{medium}.\left(\frac{d_{gap}}{d_{implemented}}\right) \tag{6}$$

A geometric visualization of a neuron sitting on top of the star-shaped electrode, as implemented in COMSOL, is depicted in (Figure 4).

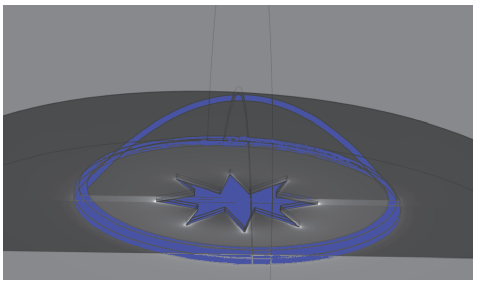

Figure 4: 3D geometry used in finite element modelling.

### 2.2.3 Electrolyte Bath

The values 1.65S/m and 80 were assigned to the conductivity and relative permittivity of the extracellular medium. It was modelled as a 60μm diameter hemisphere. The boundary of this area was considered as an electrical ground representing an electrode faraway and its potential was set to zero potential.

## 3 RESULTS

### 3.1 Passive Response under Current-clamp

Experiments were performed with three electrodes of each shape and size. Since falling voltage ramps depolarize the membrane with a lower slope than is required by rising ramps (Schoen and Fromherz, 2008), falling voltage ramps with steps of -50mV were used for the experiments. The cells were stimulated by the microelectrode arrays and the intracellular response was measured using a sharp electrode. A circular electrode with an area of 707μ$m^2$ and perimeter of 94μm caused an action potential (AP) when the stimulus exceeded -1000mV. The small, medium and large star shaped electrodes with perimeters of 106μm, 148μm, 186μm and areas of about 280$\mu m^2$, 478$\mu m^2$ and 798$\mu m^2$ all caused APs with -750mV stimuli, which is 25% less than the circular electrode. So although the large star shaped electrode has a larger area than the circular electrode, it can stimulate the cells using lower voltages.

Simulation results of intracellular response of the star-shaped electrode versus horizontal displacement from the centre of electrode, is depicted in (Figure 5).

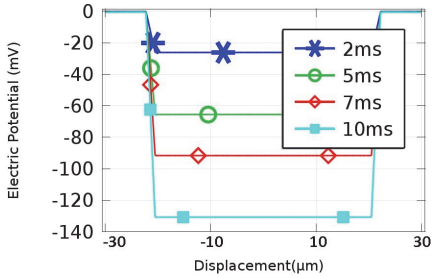


Figure 5: Intracellular Response to extracellular stimulation with falling voltage ramp of -60mv/ms and star electrode with respect to displacement from the centre, at times 2ms, 5ms, 7ms and 10ms.

Simulation results of the intracellular response due to a circular electrode with the same area as the star-shaped electrode is illustrated in (Figure 6).

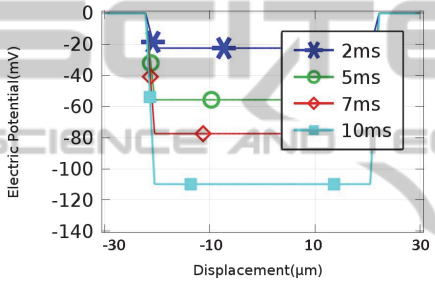


Figure 6: Intracellular response to extracellular stimulation with falling voltage ramp of -60mv/ms and circle electrode with respect to displacement from the centre, at times 2ms, 5ms, 7ms and 10ms.

As can be seen, the star electrode, results in a larger hyperpolarisation of the intracellular medium.

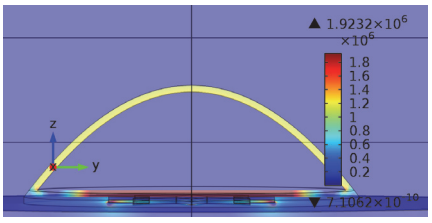

Figure 7: Electric field at different areas of the cell at the termination of stimulus voltage ramp on star electrode.

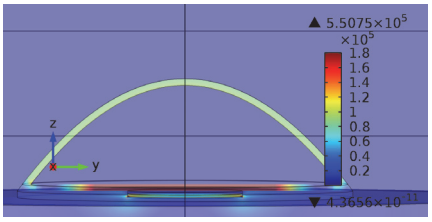

Figure 8: Electric field at different areas of the cell at the termination of stimulus voltage ramp on circular electrode.

Figures 7 and 8 show that the electric field is larger in the unattached membrane for the star-shaped electrode in comparison to the round electrode.

## 3.2 Current Density Distribution on Electrode

It has been reported that high charge density on the electrode surface can result in cell damage when these electrodes are used for stimulating parts of brain tissue (McCreery et al., 1990). With the experiments performed here it was observed that using star shaped electrodes did not cause cell death or visibly damage the individual cells. Figures 9 and 10 illustrate the current density distribution on the star-shaped electrode surface at the termination of a stimulus.

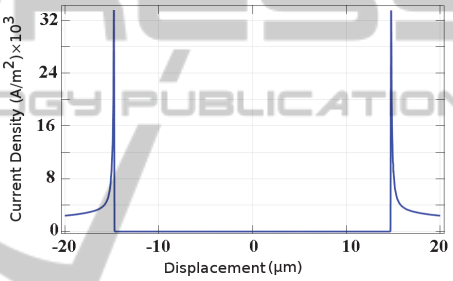


Figure 9: Current density on star electrode due to -60mV/ms falling voltage ramp stimuli, versus displacement from the centre of electrode at t=10ms.

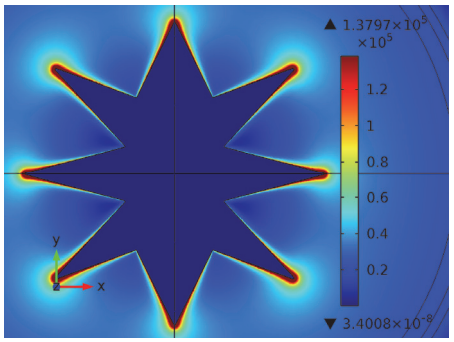

Figure 10: Current density distribution on star electrode due to -60mV/ms falling voltage ramp stimuli at t=10ms.

Figures 11 and 12 illustrate the current density distribution on the circular electrode surface at the termination of a stimulus.

As seen in figures 9 and 11, the star electrode results in a spatial non-uniformity in the current density which is almost three times that of the circular electrode. Since the activating function is proportional to the spatial derivative of current

density, larger non-uniformity results in a larger activating function and thus more effective stimulation (Wei and Grill, 2009). Furthermore, during the experiment no cell damage was observed and the threshold voltage was reduced for the star electrodes, as compared to the circular electrode.

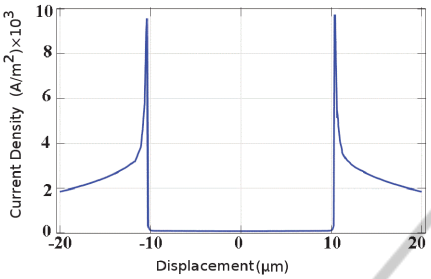


Figure 11: Current density on circular electrode due to -60mV/ms falling voltage ramp stimuli, versus displacement from the centre of electrode at t=10ms.

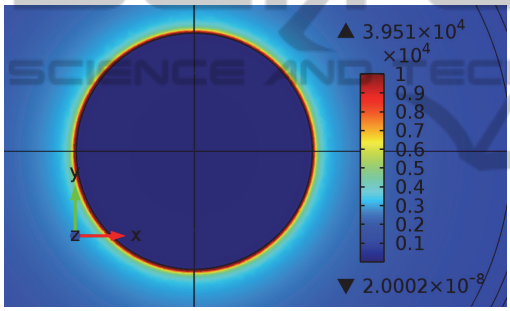


Figure 12: Current density distribution on circular electrode due to -60mV/ms falling voltage ramp stimuli at t=10ms.

The sealing resistance obtained from FEM ANALYSIS was calculated by dividing the electrode voltage by the whole current on the electrode surface while assuming that current through the cell is negligible compared to current through the sealing gap (Buitenweg et al., 1999). The sealing resistance of the star electrode at 9ms was 5GΩ while for the circular electrode it was 32.9MΩ. This shows that sealing resistance increases by changing the electrodes shape from circular to star.

### 3.3 Model Validation

The simulation results were compared with experimental data using custom made MEAs with various electrode geometries. The results of FEM ANALYSIS matched well with the experimental results. Since experimentally star-shaped electrodes were excited at lower voltages compared to round electrodes.

The experimental results showed that an action potential was triggered by smaller stimulus amplitudes when star shaped electrodes were used instead of circular electrodes. Previous studies (Buitenweg et al., 2003) show that smaller circular electrodes result in higher intracellular response. The electrode areas of two star shaped electrodes are smaller than the circular electrode and they resulted in a cell excitation with lower stimulus. However the larger star electrode which had a larger area than the circular electrode caused neuron excitation with lower stimulus amplitudes as well.

## 4 CONCLUSIONS

Circular microelectrodes with smaller radius produce a larger response to extracellular stimulation (Buitenweg et al., 2003). Serpentine electrodes in centimetre dimensions reduced the threshold voltage at higher perimeters and farther distances from the electrode (Wei and Grill, 2009). In the present study we examined the effect of sharp edges as well as perimeter and area on neuron stimulation by microelectrodes. Results show that sharp edges have a higher impact than other geometries since the medium and large star electrodes were excited by the same voltage. The model result showed that using electrodes with the same area but different perimeter and sharp edges results in larger hyperpolarisation in the cell and a higher current density, almost three times that of the round electrode, at the edges. Therefore, it would be ideal if electrodes were designed to be smaller than the neuron being investigated and also to contain sharp edges. Future work will investigate different electrode geometries, both through simulation and also via experimental study.

## ACKNOWLEDGEMENTS

The authors wish to acknowledge the research grants from the Alberta Ingenuity Fund, The Natural Sciences and Engineering Research Council of Canada (NSERC) and The Canadian Institute of Health Research (CIHR), Regenerative Medicine and Nanomedicine Program RMF 82496.

We also wish to thank the Advanced Micro/Nanosystems Integration Facility at the University of Calgary for fabricating the devices.

## REFERENCES


Buitenweg, J. R., Rutten, W. L. C. and Marani, E., 1999. 'Finite element modeling of the neuron-electrode interface', *IEEE Engineering in Medicine and Biology Magazine*, vol.19, no.6, pp. 46-52.

Buitenweg, J. R., Rutten, W. L. C., Marani, E., 2003. 'Geometry-based finite-element modeling of the electrical contact between a cultured neuron and a microelectrode', *Biomedical Engineering, IEEE Transactions on*, vol.50, no.4, pp.501-509.

Choi, C. T. M., You, S., 2012. 'Finite element models of neuron electrode sealing interfaces', *Magnetics, IEEE Transactions on*, vol.48, no.2, pp.643-646.

Cogan S. F., 2008. 'Neural stimulation and recording electrodes', *Ann. Rev. Biomed. Eng*, vol.10, pp.275-309.

Elia S., Lamberti P., Tucci V., 2009. 'A finite element model for the axon of nervous cells', *COMSOL Conference*.

Huang, X., Nguyen, D., Greve, D. W., Domach, M. M., 2004. 'Simulation of microelectrode impedance changes due to cell growth', *Sensors Journal, IEEE*, vol.4, no.5, pp. 576- 583.

Lu T. Z., Feng Z-P, 2011. 'A sodium leak current regulates pacemaker activity of adult central pattern generator neurons in *Lymnaea Stagnalis*'. *PLoS ONE,* vol.6, no.4, p.e18745.

McCreery, D. B., Agnew, W. F., Yuen, T. G., Bullara, L., 1990. 'Charge density and charge per phase as cofactors in neural injury induced by electrical stimulation'. *IEEE Trans. Biomed. Eng.*, vol.37, no.10, pp.996–1001.

Molleman A., 2003. '*Basic Theoretical Principles, in Patch Clamping: An Introductory Guide To Patch Clamp Electrophysiology*', John Wiley & Sons, Ltd, Chichester, UK.ch2.

Moulin C., Gliere A., Barbier D., Joucla S., Yvert B., Mailley P., Guillemaud R., 2008. 'A new 3-D finite-element model based on thin-film approximation for microelectrode array recording of extracellular action potential' *IEEE Trans. Biomed. Eng.*, Vol.55, pp.683-92.

Rutten, W. L. C. 2002. *Annu. Rev. Biomed. Eng*. 4, 407.

Schoen I, Fromherz P., 2007. 'The mechanism of extracellular stimulation of nerve cells on an electrolyte-oxide-semiconductor capacitor'. *Biophys. J.,* 92, vol.92, no.3, pp.1096–1111.

Schoen, I., Fromherz, P., 2008. 'Extracellular stimulation of mammalian neurons through repetitive activation of Na+ channels by weak capacitive currents on a silicon chip'. *J Neurophysiol,* vol.100, no.1, pp.346–357

Syed, N. I., Zaidi, H., Lovell, P., 1999. U. Windhorst, H. Johansson (Eds.),' *Modern Techniques in Neuroscience* Research', Springer, Berlin, Heidelberg , pp. 361–377.

Wei X. F., Grill W. M., 2009. 'Analysis of high-perimeter planar electrodes for efficient neural stimulation'. Front. *Neuroeng*. , vol.2, no.15.

Yúfera, A., Olmo, Daza, P and Cañete, D. A., 2003. '*Basic Theoretical Principles, in Patch Clamping: An Introductory Guide To Patch Clamp Electrophysiology*', John Wiley & Sons, Ltd, Chichester, UK. ch2.